Available online at www.CivileJournal.org

Civil Engineering Journal

(E-ISSN: 2476-3055; ISSN: 2676-6957)

Vol. 12, No. 02, February, 2026

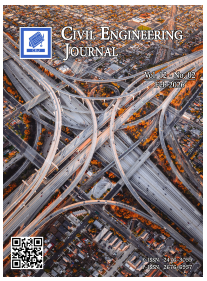

Performance Evaluation and Model of GFRP Reinforced Concrete Filled GFRP Tube Column Under Accelerated Aging

Woraphot Prachasaree [1*], Jakrawa Ouiseng [2], Abideng Hawa [3], Pong-in Intarit [1], Ornkamon Wangapisit [1], Suchart Limkatanyu [1]

[1] *Department of Civil and Environmental Engineering, Faculty of Engineering, Prince of Songkla University, Hat Yai 90110, Thailand.*

[2] *Large Scale Irrigation Construction Office, Royal Irrigation Department, Ministry of Agriculture and Cooperatives, Bangkok, Thailand.*

[3] *Infrastructure and Materials Innovation Research Unit, Department of Civil Engineering, Princess of Naradhiwas University, Narathiwat 96000, Thailand.*

Received 29 May 2025; Revised 16 January 2026; Accepted 20 January 2026; Published 01 February 2026

Abstract

Conventional reinforced concrete structures exposed to aggressive environments show a risky tendency toward performance degradation due to concrete deterioration and reinforcement corrosion. Consequently, the use of fiber-reinforced polymer (FRP) materials in concrete structures as one of the alternative potential materials for mitigating serious durability issues in structural applications has gained increasing acceptance. The study aims to evaluate the performance and durability of GFRP-reinforced concrete-filled GFRP tube columns under accelerated aging. Three different column specimens, 1) GFRC-F-GFT, 2) GFRC, and 3) C-F-GFT, were immersed under water at 80°C for 12 hrs (wet phase), followed by specimen placement above water at ambient room temperature for 12 hrs (dry phase) in each aging cycle. The behavior and performance of the specimens were experimentally investigated through uniaxial compressive loading. The experimental results were evaluated to develop a strength capacity model that incorporated the environmental exposure effect through the strength reduction factors (C_0, η_1, and η_2). To establish the correlation between accelerated and natural aging, field investigation data under the tropical marine environment and the simplified time-invariant model were utilized to predict structural performance. Based on this study, the GFRC-F-GFT specimen degradation under accelerated wet-dry aging at 290 cycles can reduce axial column capacity up to 50%, which is equivalent to the predicted degradation under a natural tropical marine environment over 50 years.

Keywords: Column; Concrete; Fiber Reinforced Polymer; Durability; Degradation; Aging.

1. Introduction

The deterioration of conventional reinforced concrete structures is one of the most deleterious problems in infrastructure and various other fields of construction. The corrosion of conventional steel reinforcement can initiate excessive cracks and deflection, which eventually lead to diminished structural performance, serviceability, and durability. At present, fiber-reinforced polymer (FRP) composites, such as FRP rebars, wrapping systems, and FRP sections, have been progressively implemented and have gained widespread acceptance as effective alternatives. In particular, the use of glass fiber-reinforced polymer composites for both longitudinal and lateral reinforcement in compression structural members has been widely carried out and presented in many recent works [1-7]. However, using

* Corresponding author: woraphot.p@psu.ac.th

https://doi.org/10.28991/CEJ-2026-012-02-013

only internal GFRP reinforcement as the main reinforcement in concrete compression members has not been permitted in practice under most of the widely recognized guidelines and standard codes of practice. To mitigate reinforcement corrosion issues and improve structural performance under compression, the use of combined internal and external reinforcement of concrete members, such as concrete-filled FRP sections, has been developed and implemented for applications such as bridge piers, piles, etc., in marine environments [8-10].

Over the past decade, applications of concrete-filled FRP tubes have gained the attention of numerous researchers and professional engineers. More recent research has focused on traditional concrete-filled FRP tubes, investigating experimental behavior and analytical models, while also exploring manufacturing techniques for FRP tubes [11]. The behavior of concrete-filled FRP tubes (CFFTs) has been extensively studied and reported in the literature, with a focus on compressive strength, confinement, and ductility in short-term responses [8-9, 12-16]. The axial load capacity model based on the superposition principle of the reinforced concrete-filled GFRP pultruded tubular column (RCFGPT**)** with internal steel spiral stirrup was proposed and validated through experimental results [17]. The hybrid structure systems of seawater sea sand concrete (SWSSC)-filled FRP tubes have been experimentally investigated for the durability issue under artificial seawater environments for 6 months [18]. The impact of tube thickness on the residual compressive strength of innovative SWSSC-filled hybrid carbon-glass FRP tubes was examined under accelerated alkaline and seawater conditions. Based on the developed predictive model, the knockdown factors of about 0.6-0.8 and 0.7-0.8 were recommended for cross-ply and hoop tubes, respectively [19]. Saadeh & Irshidat [20] studied the compression behavior of concrete-filled filament-wound FRP tubes. The results showed that the performance of concrete-filled FRP tubes was significantly affected by the FRP thickness [20]. Elkafrawy et al. [21] mentioned that current design codes and standards underestimate the contribution of GFRP rebars to compressive column capacity. New predictive models and design provisions that accurately represent the compressive strength contribution of GFRP reinforcement are needed. In addition, advanced studies on the long-term durability of GFRP-reinforced structures under various environmental conditions are still lacking [21]. As mentioned earlier, nearly all previous studies have been published on the performance and behavior of concrete-filled FRP tubes (CFFTs) over short-term periods. Durability studies on concrete-filled FRP tubes (CFFTs) are rather lacking compared to other FRP composites [22].

In general, the structural conditions of infrastructure would demand a high degree of performance with acceptable long-term durability. However, there is currently limited research and data on durability aspects, particularly over long periods under natural and accelerated conditions. This study aims to evaluate the structural performance and the behavior of GFRP-reinforced concrete-filled FRP tubes (CFFTs) under an accelerated wet-dry aging process. The correlation between accelerated and natural tropical marine exposure environments was evaluated using field investigation data and the predicted performance model. Three different concrete column specimens subjected to accelerated aging conditions were experimentally investigated under uniaxial compression. Based on the experimental results, the predicted strength model was proposed herein. Using field-collected data (natural aging under a tropical marine environment), the long-term structural performance was evaluated through the simplified time-invariant model. Finally, the correlation between accelerated and natural aging was developed using analytical results. The methodology used in this study is summarized and illustrated in Figure 1. The findings are expected to partially bridge this knowledge gap, contributing to the understanding of proposed design recommendations, structural behavior, and performance through the experimental investigation herein.

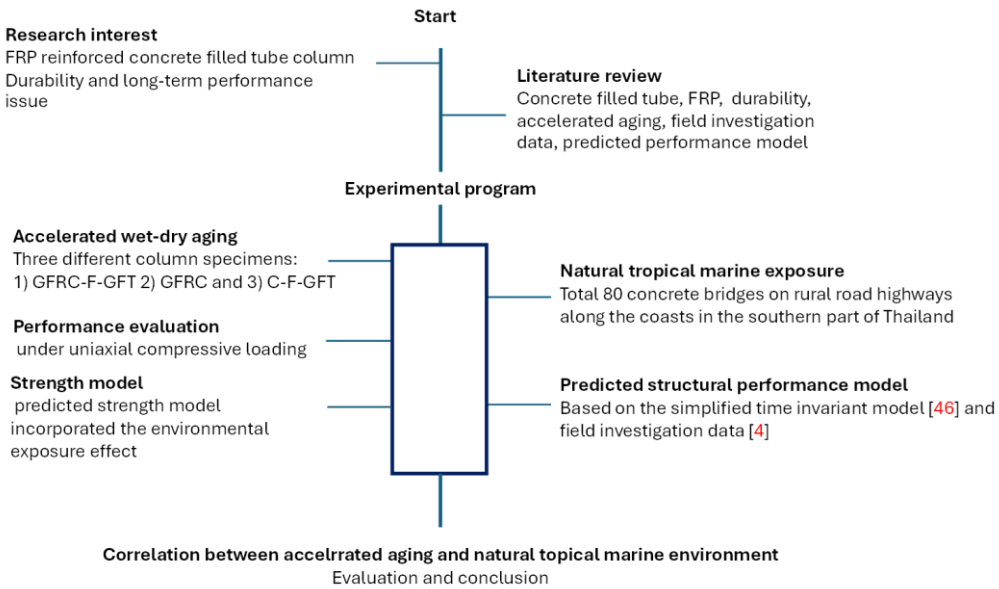

Figure 1. Summary of the research methodology

2. Experimental Program for Accelerated Aging

As shown in Figure 1, the predicted structural performance under natural tropical marine conditions, along with the correlation between accelerated and natural aging, is evaluated based on a simplified time-invariant model and field investigation data, which will be discussed in Section 6 later. To evaluate structural behavior and performance when exposed to the accelerated aging condition, the GFRP reinforced concrete-filled GFRP tube columns (GFRC-F-GFT) were experimentally examined under axial compression loading in this study. The details of specimen series, materials, and aging schemes are discussed below.

2.1. Column Specimens

A total of 27 circular column specimens were prepared and cast with a diameter of ~125 mm. The nominal specimen length was 500 mm for all columns, resulting in a height to diameter ratio of about 4.0. All test specimens were wet cured at room temperature for 28 days before undergoing the process and subsequent aging testing. The column specimens were classified into three categories: 1) GFRP reinforced concrete-filled GFRP tube column (GFRC-F-GFT), 2) GFRP reinforced concrete without FRP tube column (GFRC), and 3) Concrete-filled GFRP tube column without internal GFRP rebars (C-F-GFT), as shown in Figure 2. For all FRP reinforced concrete specimens (GFRC-F-GFT and GFRC), the specimens were internally reinforced with four 10 mm-diameter GFRP rebars without lateral reinforcement. The longitudinal reinforcement ratio (ρ_{frp}) was equal to 2.5%. However, the additional lateral reinforcement (6 mm-diameter steel circular ties) was tied at specific spacing along one-fifth of the specimen length from both specimen ends to avoid and prevent premature failure in the end zones. The characteristics of all specimens are summarized in Table 1.

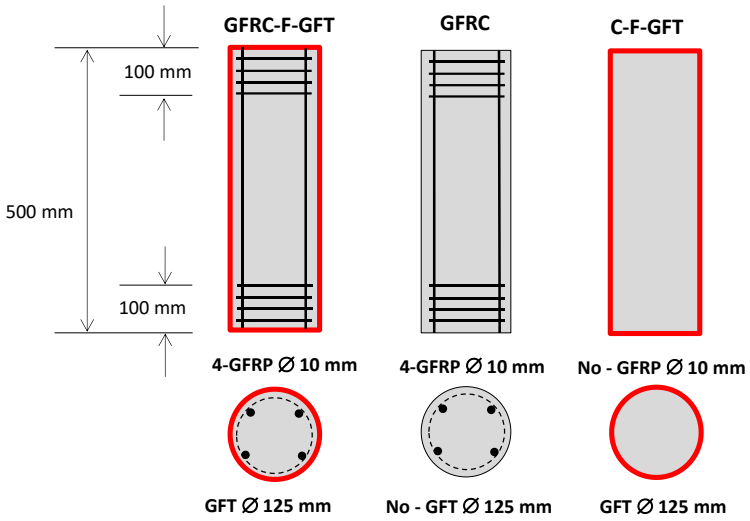

Figure 2. Details of column specimens

Table 1. Characteristics of the test specimens

Group No.	Sample label	Tube	Column		Reinforcement	ρ_{frp} (%)	f'_c (MPa)
			Length (mm)	Diameter (mm)			
C-1	GFRC-F-GFT	GFRP	500	125	GFRP rebar	2.48	41.8
C-2	GFRC	-	500	125	GFRP rebar	2.48	41.7
C-3	C-F-GFT	GFRP	500	125	-	-	42.1

For concrete used, the average cylindrical compressive strength (f'_c) at 28 days of age was evaluated to be 41.7 MPa for GFRC-F-GFT and GFRC specimens, and 42.1 MPa for C-F-GFT specimens. At both end zones of all test specimens, 6 mm-diameter steel round rebars (grade SR24 – yield strength of 240 MPa) were used for column circular ties with a spacing of 50 mm. Glass fiber-reinforced polymer (GFRP) rebars, 10 mm in diameter, were provided as the main longitudinal reinforcement for the GFRC-F-GFT and GFRC specimens. According to supplier data, the tensile strength of the GFRP rebars was 735 MPa. However, previous research studies conducted on the compressive responses of FRP rebars have been limited and therefore the data are not widely available [23]. Based on previous studies, the compressive strength of FRP rebars is significantly lower than the tensile strength with reductions varying from 50% to 70% [24-26]. The axial compressive load contribution by the longitudinal GFRP rebars varied between 5 and 10 percent of the maximum axial compression capacity. Thus, the axial compressive capacity contributed by longitudinal GFRP reinforcement can be considered negligible for compression members design purposes [3]. In recent research, the compressive strength contribution of FRP rebars based on the previous research data of 269 specimens was proposed

for 2 percent of their tensile strength [16]. In addition, GFRP circular tubes for the column specimens (GFRC-F-GFT and C-F-GFT) were produced by a filament winding process using E-glass fiber and epoxy as reinforcement and matrix, respectively. The fiber orientation was laid at ± 45° relative to the longitudinal direction of the GFRP circular tubes. The circumferential and compressive strengths of the GFRP circular tube were 255 MPa and 85 MPa, respectively.

2.2. Aging Scheme

The column specimens were aged under the accelerated wet/dry process for 80 and 160 cycles before undergoing uniaxial compressive testing. The experimental results of the aged columns were evaluated and compared to the experimental results of the unaged column (control specimens). Each accelerated wet/dry cycle consisted of the following steps as follows: 1) The column specimens were immersed in water at 80 ± 5 ºC for 10 hours. 2) A transition period of 2 hours followed before the dry phase. During this transition, the column specimens remained inside the temperature bath, with the water entirely drained out. 3) For the dry phase, the column specimens were exposed to the ambient environment for 10 hours. 4) This was followed by water immersion at 80 ± 5 ºC during 2 hours of the transition period before the next cycle. The water temperature during the wet phase was maintained at a constant level throughout the immersion period. A summary of the accelerated aging process is illustrated in Figure 3.

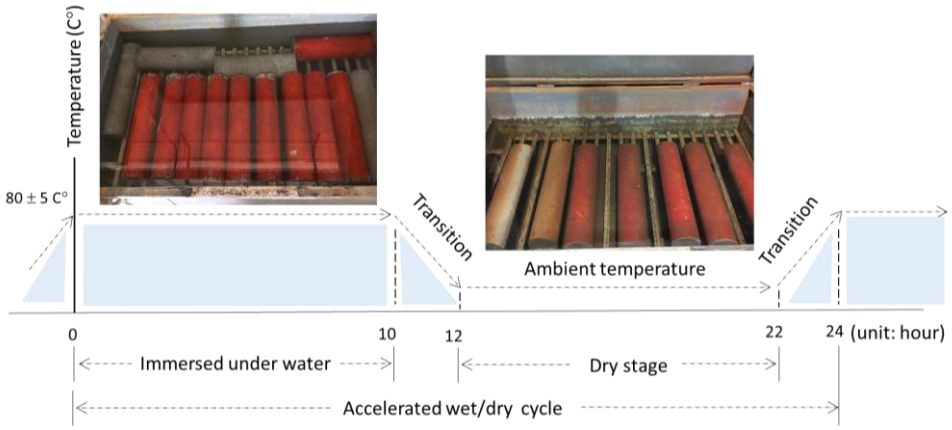

Figure 3. Accelerated aging scheme (wet-dry cycles)

3. Experimental Test Set-Ups

All column specimens were experimentally tested under uniaxial compression loading. To investigate their structural responses and performances, sensors were used. Linear variable differential transducers (LVDTs) with 150 mm gauge length were placed on the rigid steel floor of a universal testing machine to monitor the axial deformation of the column specimens. Strain gauges were attached at three different positions on the outer surface of each column specimen, while two strain gauges were mounted on the GFRP rebars for the GFRC-F-GFT and GFRC specimens. For experimental preparation, the column specimen was arranged on an adjustable steel ball support positioned between the top and bottom rigid steel floors of the universal testing machine. To conduct the monotonic compressive test, a uniaxial compressive load was applied through a rigid steel plate over the adjustable ball support, ensuring the even distribution of the compression load across the tested specimen. The applied loads, deformations and strain responses were monitored and recorded through attached sensors connected to a data acquisition system. The test set-up is schematically illustrated in Figure 4.

Figure 4. Test set-ups and instruments

4. Experimental Results

The experimental investigation into the performance and durability of GFRP reinforced concrete-filled GFRP tube columns was conducted through uniaxial compression load testing as described in Section 2. The experimental results along with aging duration, maximum compressive strength, the ratio of confined column strength (f'_{cc}) to unconfined and unaged concrete strength (f'_c), and the column axial strain are presented in Table 2. In general, the normalized confined concrete strength (f'_{cc}/f'_c) of unaged test specimens was higher than that of test specimens subjected to accelerated wet-dry aging cycles. As expected, the average ratio (f'_{cc}/f'_c) values gradually decrease with an increasing number of aging cycles. During aging, the degradation of the GFRP tube and internal GFRP reinforcement (rebars) was influenced by material damage due to the coupled thermal-hydro-mechanical cyclic effect (expansion-contraction). Eventually, the significant loss in GFRP tube stiffness led to a specific deterioration in strength, falling considerably below its material strength. The average strength losses of aged column GFRC-F-GFT specimens were determined to be 15% and 22% compared to unconditioned column strength for 80 and 160 wet-dry cycles, respectively. The percentage difference in strength loss varied between 9% and 17% for column specimens without the GFRP tube (GFRC) exposed to aging conditions during 80 to 160 cycles. However, it was found that the average strength loss in aged GFRC column specimens remained approximately 16% after 80 cycles of accelerated wet-dry aging.

Table 2. Experimental test results

Sample	Wet-dry cycles	No.	ρ_{frp} (%)	Tube	@ Maximum compressive		f'_{cc}/f'_c	Maximum axial strain	Axial $\varepsilon_l/\varepsilon_{l0(avg)}$	Hoop $\varepsilon_h/\varepsilon_{h0(avg)}$
					Strength (kN)	Stress (MPa)		(GFT) (mm/mm)	(GFT)	(GFT)
GFRC-F-GFT	-	1	2.48	GFRP	640	50.4	1.21	1870	-	-
		2			635	50.0	1.20	1720		
		3			648	51.0	1.22	2185		
GFRC	-	1	2.48	-	447	37.6	0.90	-	-	-
		2			439	36.9	0.88			
		3			448	37.6	0.90			
C-F-GFT	-	1	-	GFRP	598	47.1	1.12	1780	-	-
		2			594	46.8	1.11	2256		
		3			608	47.9	1.14	2230		
GFRC-F-GFT	80	1	2.48	GFRP	550	43.3	1.04	1710	0.888	0.973
		2			539	42.4	1.02	1680	0.873	
		3			542	42.7	1.02	1625	0.844	
GFRC	80	1	2.48	-	415	34.9	0.84	-	-	-
		2			389	32.7	0.78			
		3			405	34.0	0.82			
C-F-GFT	80	1	-	GFRP	504	39.7	0.94	2310	1.106	0.899
		2			523	41.2	0.98	1820	0.871	
		3			527	41.5	0.99	1785	0.854	
GFRC-F-GFT	160	1	2.48	GFRP	502	39.5	0.95	1665	0.865	0.934
		2			492	38.7	0.93	2020	1.049	
		3			510	40.2	0.96	1846	0.959	
GFRC	160	1	2.48	-	376	31.6	0.76	-	-	-
		2			371	31.2	0.75			
		3			364	30.6	0.73			
C-F-GFT	160	1	-	GFRP	497	39.1	0.93	1372	0.657	0.886
		2			489	38.5	0.91	1405	0.673	
		3			487	38.3	0.91	1388	0.664	

The load and displacement relation of GFRC-F-GFT and C-F-GFT column specimens is different from that of GFRC column specimens due to the absence of external confinement (the GFRP tube). Typically, displacement increases significantly when increasing the applied load until reaching maximum load capacity in conventional reinforced concrete column and GFRC column specimens. However, the load-displacement slope (column stiffness) of GFRC-F-GFT and C-F-GFT column specimens was changed abruptly due to damage accumulation in the external confinement (GFRP tube). After this point, displacement gradually increases until internal longitudinal reinforcement (GFRP rebars)

buckled, followed by sudden concrete crushing and GFRP tube rupture (tearing out). The load-displacement relationship in an abrupt failure with the total loss of column capacity is shown in Figures 5 and 6. A bilinear load and displacement relationship was observed in most test specimens. For GFRC column specimens, it was found that the load-displacement behavior closely resembled that of GFRP reinforced concrete with lateral reinforcement [4]. In these specimens, the linear load-displacement relation was maintained until reaching maximum load capacity of column specimens. Upon GFRP rebars buckling and the crushing of concrete surrounding the rebars, longitudinal cracks rapidly widened, followed by sudden failure of the column specimen. After accelerated wet-dry aging, the load-displacement response remained consistent in the pre-aging manner. It was observed that the failure mode of all aged specimens did not significantly change. However, the GFRP tube and rebars exhibited rupture and buckling at a lower ultimate capacity due to material degradation.

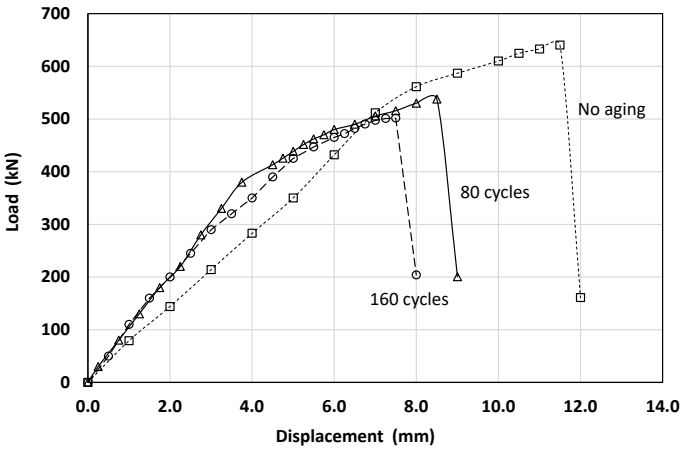

(a) Specimens: GFRC-F-GFT

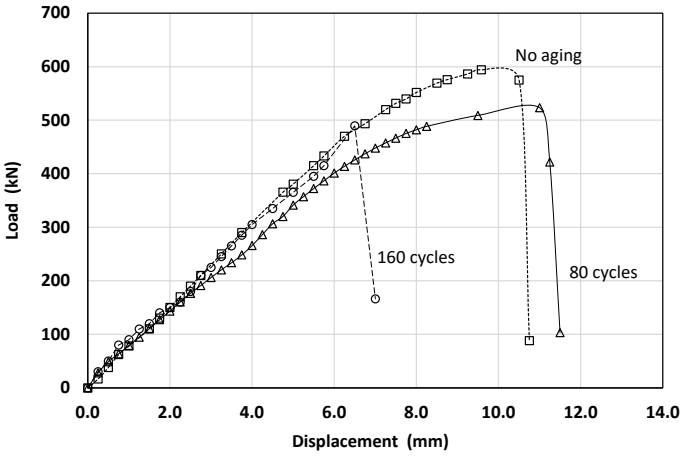

(b) Specimens: GFRC

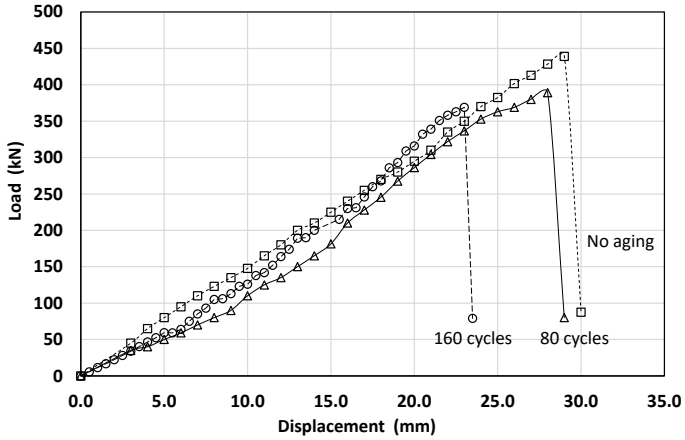

(c) Specimens: C-F-GFT

Figure 5. Relationship between load and displacement

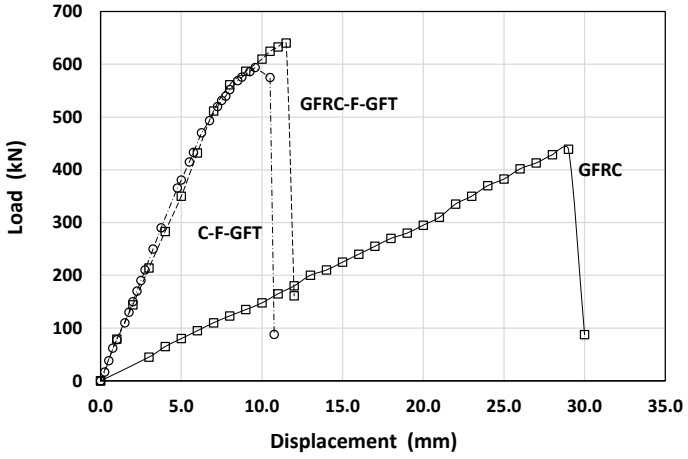

(a) Specimens: no aging

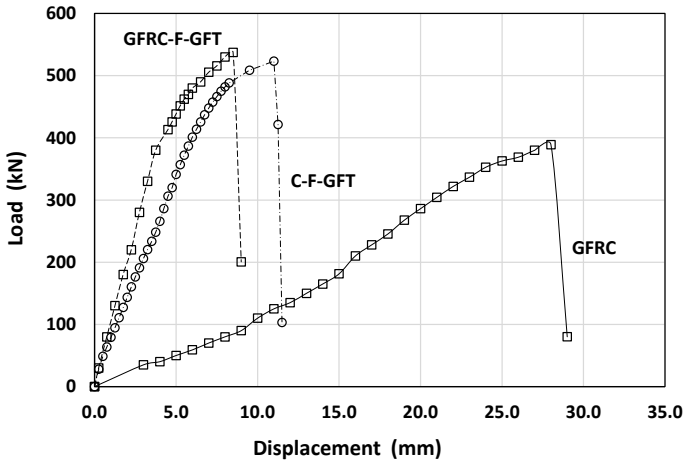

(b) Specimens: 80 cycles of aging process

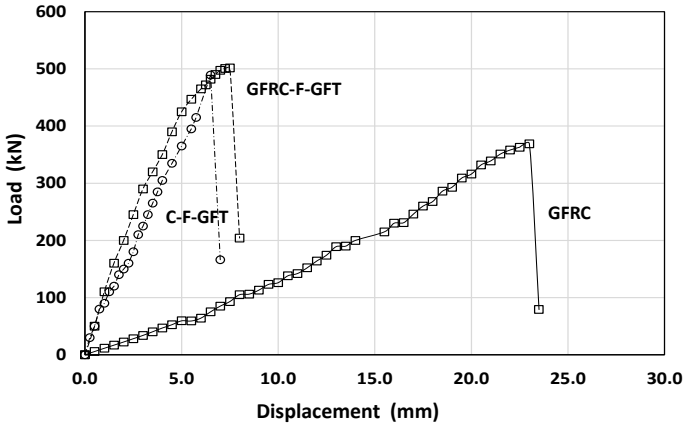

(c) Specimens: 160 cycles of aging process

Figure 6. Relationship between load and displacement

The typical load and lateral strain (ε_h) relations of tested specimens are presented in Figure 7. Lateral strains were measured using stain gauges mounted on the GFRP tube, though GFRP tube surface damage from rupture and local bucking may have led to lower data accuracy. Similar to the load-displacement relation, the relationship of load and lateral strain followed an identical pattern. The lateral strength reduction in GFRC-F-GFT and C-F-GFT column specimens was consistent as mentioned in previous studies [27, 28]. Due to the lateral strength reduction, the ratio of average lateral strain (unaged to aged specimens) decreases slightly with increasing aging cycles. To characterize the post-elastic behavior of test specimens, the deformability factor is used to indicate the post-elastic behavior of FRP reinforced structural members. In general, it is defined as the ratio of energy absorption at the ultimate state to that at a specific deformation in the ascending portion of the load-deformation relation. Compared to the ductility factor, the

deformability factor provides a more appropriate characterization based on energy absorption [4]. In this study, the post-elastic point defined as 85% of maximum load capacity in the descending portion was designated as the ultimate point. Also, the deformation point at maximum load capacity in the ascending portion was selected to be the limiting deformation point. The average deformability factor was determined as 1.055 for both GFRC-F-GFT and C-F-GFT specimens, and 1.015 for GFRC specimens.

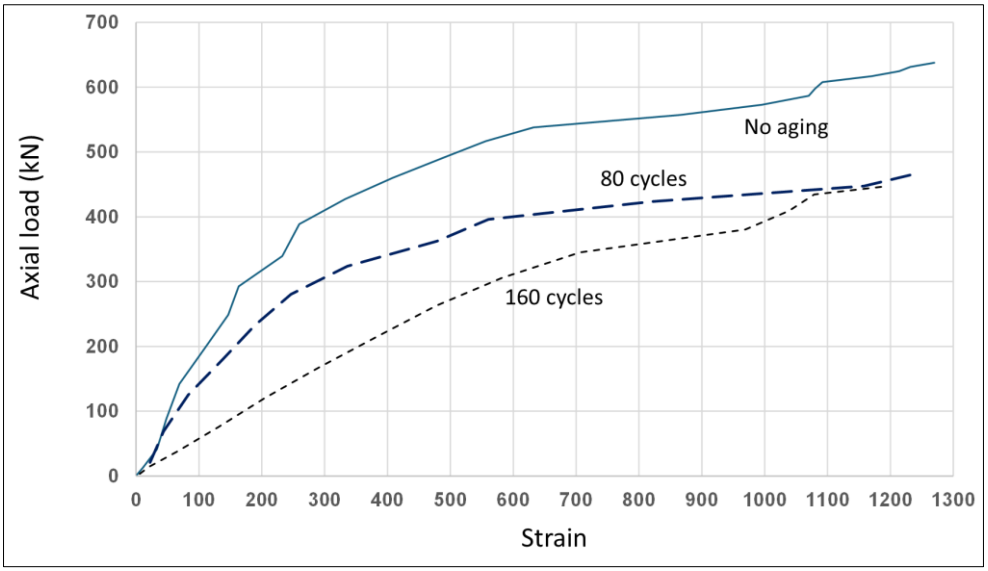

(a) Specimens: GFRC-F-GFT

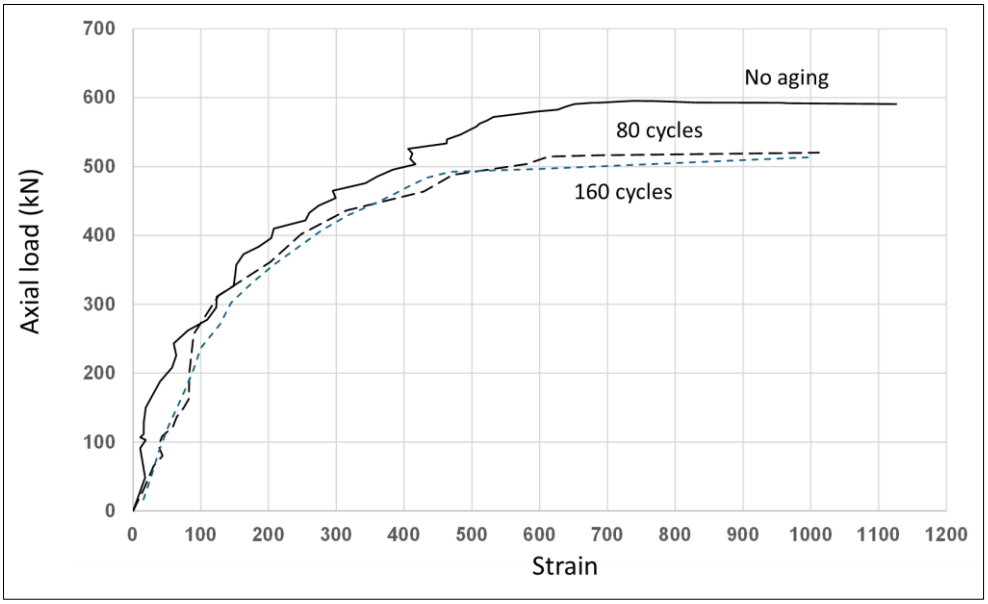

(b) Specimens: GFRC

Figure 7. Relationship between load and lateral strain on GFRP tubes

5. Strength Model

The maximum strength capacity of a short concrete column under axial loading is typically assessed based on the interactions between the concrete, longitudinal reinforcement, and confinement under specific environment conditions. For GFRP reinforced concrete columns (GFRC), various column strength models have been developed in previous studies [3, 16, 29, 30]. In addition, the prediction models by several standard codes were proposed and suggested as follows:

ACI 318-08 [31]: $$P_n = 0{,}85f_c'(A_g - A_s) + f_y A_s \quad (1)$$

ACI 318-11 [32]: $$P_n = 0{,}85f_c'(A_g - A_s) \quad (2)$$

CSA S806-12 [33]: $$P_n = \beta_1 f_c'(A_g - A_s)\ ;\ \beta_1 = 0.85 - 0.0015f_c' \geq 0.67 \quad (3)$$

AS 3600 [34]: $$P_n = 0.85f_c'(A_g - A_{frp}) + 0.0025E_{frp}A_{frp} \quad (4)$$

where, A_g and A_s are the cross-sectional area of the column and steel rebars, respectively. A_{frp} is the FRP cross-sectional area. E_{frp} is elastic modulus of FRP reinforcement. f_{fp} is the tensile strength of FRP reinforcement.

All the proposed strength models are given in the original form of short steel reinforced concrete columns under uniaxial loading. For the compressive strength of confined concrete, numerous prediction models were developed and proposed by the previous comprehensive reviews and studies over the last few decades [3, 16, 35-41]. The general form of the concrete confined strength (f'_{cc}) model is presented as follows [41]:

$$\frac{f'_{cc}}{f'_{co}} = C_1 + k_1 \frac{f'_{lu}}{f'_{co}} \quad (5)$$

where, C_1 and k_1 are calibration constants and strength enhancement coefficients for FRP confined concrete, respectively. f'_{lu} is the lateral confining pressure by FRP confinement at ultimate. f'_{co} is the maximum unconfined concrete stress.

The lateral confining pressure at rupture of the FRP tube or jacket is simply defined by Lam & Teng [36].

$$f'_{lu} = \frac{2E_{frp}t_{frp}\varepsilon_{rup}}{D} \quad (6)$$

where, E_{frp} and t_{frp} are the elastic modulus and thickness of FRP confinement, respectively. ε_{rup} is the hoop rupture strain of FRP confinement. D is the diameter of the concrete core.

Raza et al. (2021) [16] proposed the suggested strength model with R^2 and RMSE = 0.18. The strength model was evaluated through large experimental data of 500 specimens.

$$k_1 f'_{lu} = 5\, f'^{\,0.27}_{co} \left[\frac{E_{frp}t_{frp}\varepsilon_{rup}}{D}\right]^{0.73} \quad (7)$$

where, f'_{lu} is the lateral confining pressure by FRP confinement at ultimate. f'_{co} is the maximum unconfined concrete stress. k_1 is the strength enhancement coefficient for FRP confined concrete, and E_{frp} and t_{frp} are the elastic modulus and thickness of FRP confinement, respectively. ε_{rup} is the hoop rupture strain of FRP confinement. D is the diameter of the concrete core.

In general, glass fiber-reinforced polymers are hydrophilic and sensitive to water, high alkalinity, and thermal exposure. Polymers could be plasticized and expanded due to moisture absorption. The plasticization of polymers affects several mechanical and chemical properties such as stiffness, strength, and transition temperature, etc. Additionally, the fiber surfaces are covered by an accumulation of cement hydration products, leading to hydroxylic attack on the fiber surfaces, eventually resulting in surface pitting and weight loss [42]. For FRP materials exposed to prolonged elevated temperatures, the energy contributed to reactions between the polymer matrix and free oxygen can result in cracking and degradation [43]. According to durability issues and deterioration, knock down factors for environmental exposures have been provided to account for the degradation effects on mechanical properties in FRP materials by standard codes such as ACI 440.2R.2017 [44] and CAN/CSA-S6-00.R2005 [45]. The factor is typically referred to as an environmental strength reduction (C_E) as follows:

$$f_{fu} = C_E f^*_{fu} \quad and \quad \varepsilon_{fu} = C_E \varepsilon^*_{fu} \quad (8)$$

where, f_{fu} and ε_{fu} are the tensile strength and strain of FRP materials under aging condition, respectively. f^*_{fu} and ε^*_{fu} are the tensile strength and strain of unaged FRP. C_E is the reduction factor due to the environment.

Typically, the strength models of short column members are conventionally adopted in a combination of strengths provided by different materials. For GFRP reinforced concrete-filled GFRP tube columns (GFRC-F-GFT), the column strength is contributed by three different parts as 1) concrete core, 2) main internal FRP rebars, and 3) external FRP tube as follows:

$$P_n = 0.85f_c'(A_g - A_{frp}) + \beta_1 f_{frp}A_{frp} + (\beta_2 k_1 f'_{lu})A_g \quad (9)$$

where, β_1 and β_2 are the reduction factors for axial column strength due to longitudinal FRP rebars and the FRP tube, respectively. k_1 is the strength enhancement coefficient for FRP confined concrete. f'_{lu} is the lateral confining pressure by FRP confinement at ultimate. A_g is the cross-sectional area of the column. A_{frp} is the FRP cross-sectional area.

The strength reduction factors due to environmental exposure are provided as multipliers in Equation 8. Accordingly, the strength model under aging conditions can be expressed in the following typical form:

$$P_n = C_1\left[0.85f_c'(A_g - A_{frp}) + \beta_1 f_{frp}A_{frp}\right] + C_2(\beta_2 k_1 f'_{lu})A_g \quad (10)$$

where, C_1 and C_2 are the reduction factors due to the environment exposures for GFRC (GFRP rebar reinforced concrete column) and the FRP tube, respectively. k_1 is the strength enhancement coefficient for FRP confined concrete. f'_{lu} is the lateral confining pressure by FRP confinement at ultimate. A_g is the cross-sectional area of the column. A_{frp} is the FRP cross-sectional area.

To assess strength reductions over aging periods, the reduction factors due to the environment exposure, longitudinal FRP rebars, and the FRP tube are incorporated and given in the general form of the strength model as shown below:

$$P_n = C_0 0.85 f'_c \left(A_g - A_{frp}\right) + \eta_1 f_{frp} A_{frp} + \eta_2 f'_{lu} A_g \tag{11}$$

where, C_0 is the strength reduction factor due to the aging condition for the concrete column, η_1 and η_2 are the strength reduction factors due to the aging condition for longitudinal FRP rebars and the FRP tube, respectively. f'_{lu} is the lateral confining pressure by FRP confinement at ultimate. A_g is the cross-sectional area of the column. A_{frp} is the FRP cross-sectional area. f_{fp} is the tensile strength of FRP reinforcement.

From the experimental results in Table 2, the relations between the ratio (f'_{cc}/f'_c) and aging cycles for both GFRC-F-GFT and C-F-GFT column specimens were fitted using exponential regression analysis as shown in Figures 8 and 9. To evaluate the reduction coefficient η_2 for the strength model in Equation 11, the confinement effectiveness due to GFRP tubes can be determined by subtracting the unconfined strength ratio of C-F-GFT column specimens from the maximum confined strength ratio of GFRC-F-GFT column specimens. Similarly, the reduction coefficient η_1 was calculated from the difference between the maximum confined strength ratio of GFRC-F-GFT column specimens and the maximum confined strength ratio of GFRC column specimens.

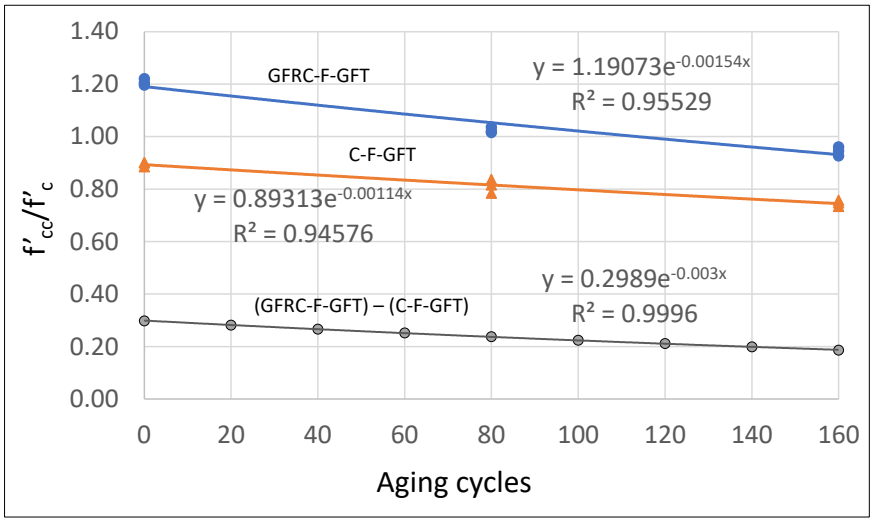

Figure 8. Confinement effectiveness (subtraction the f'$_{cc}$/f'$_c$ ratio between GFRC-F-GFT specimens and C-F-GFT specimens)

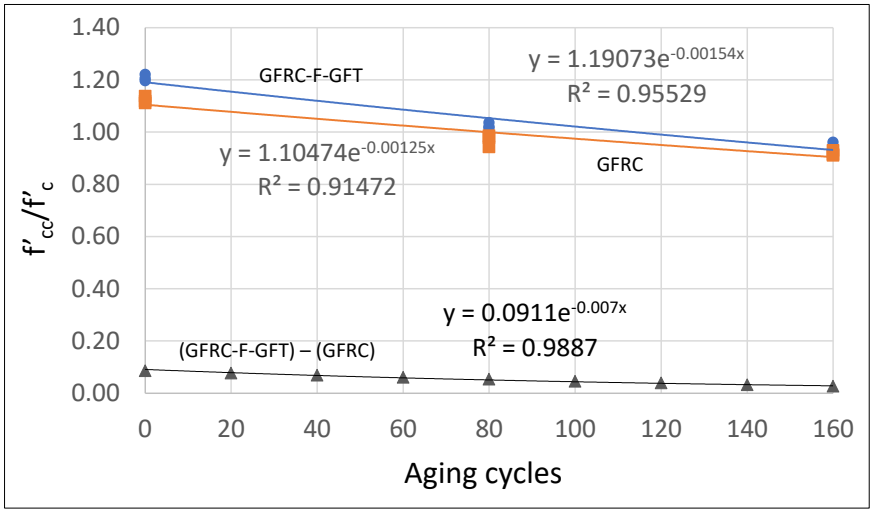

Figure 9. Longitudinal reinforcement effectiveness (subtraction the f'$_{cc}$/f'$_c$ ratio between GFRC-F-GFT specimens and GFRC specimens)

For the strength reduction C_0, the value was directly determined using Equation 11 and Table 2. A linear regression analysis was performed to evaluate the concrete column strength over aging duration as shown in Figure 10. Then, the strength reduction corresponding to FRP parts (η_1 and η_2) as shown in Figures 8 and 9 was subsequently transformed into retention form. The reduction coefficients η_1 and η_2 were obtained from curve fitting of the retention values over aging duration. Thus, the proposed strength reduction factors incorporating degradation effects from accelerated wet-dry cycles can be represented as follows (see Figure 11):

$$C_0 = 1 - 0.0006N \quad (12.1)$$

$$\eta_1 = 1 - 0.0045N \quad (12.2)$$

$$\eta_2 = 1 - 0.0024N \quad (12.3)$$

where, N is the number of accelerated wet-dry cycles.

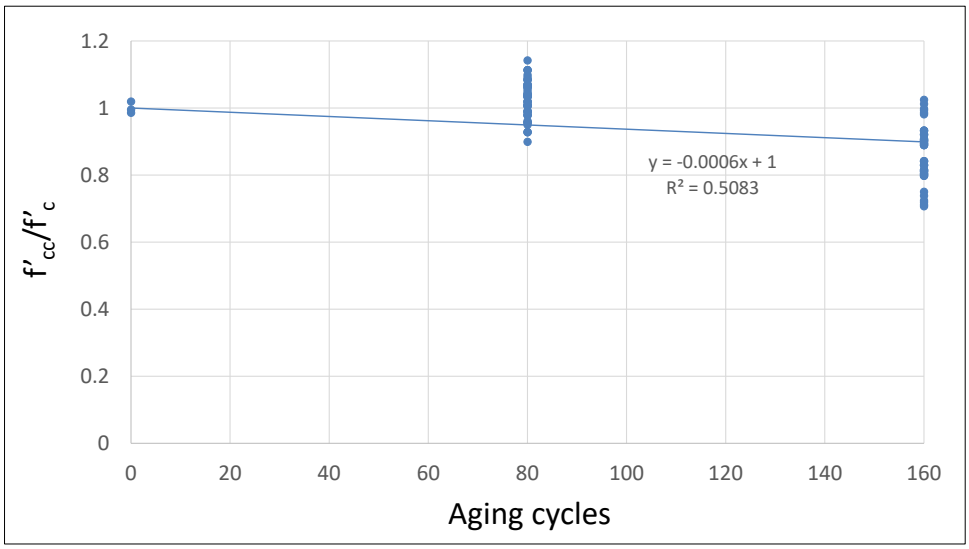

Figure 10. Reduction of concrete strength by varying aging duration

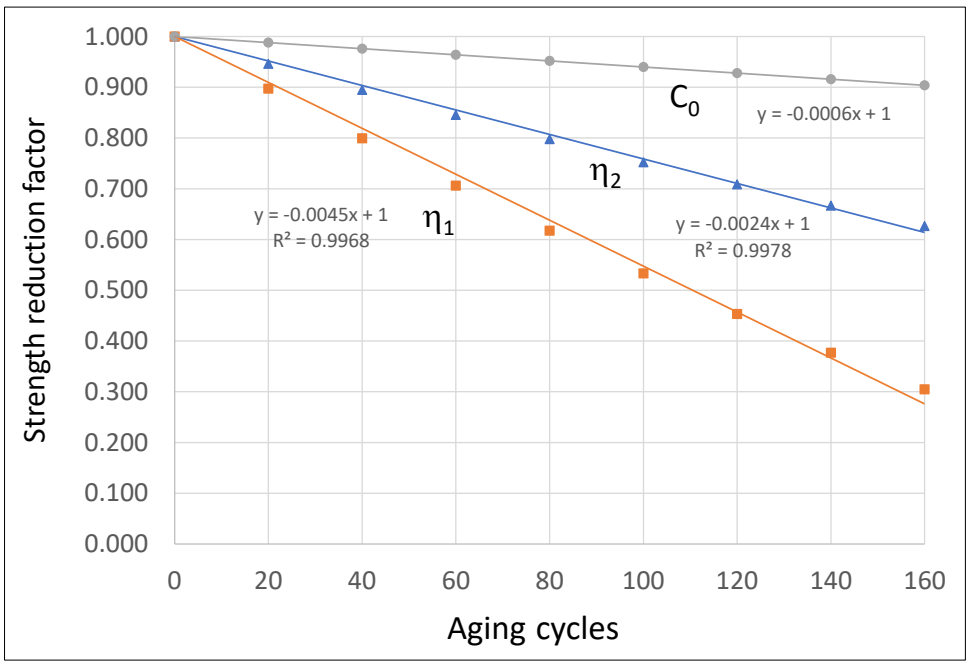

Figure 11. Strength reduction factors varying by aging duration (C_0, η_1 and η_2)

6. Correlation with Field Investigation Data

The correlations for the relationship between aging duration and strength reduction are commonly used for aging analysis. In this study, the structural performance at a specific strength retention under an accelerated wet-dry process was correlated through the predicted results based on field investigation data at other strength retention values. The field investigation data of a total of 80 concrete bridges exposed to the tropical marine environment on rural road highways along the eastern and western coasts of southern Thailand were collected as part of a research program initiated by the Department of Rural Roads (DDR) in early 2014 to study important issues influencing bridge performance [46]. In the tropical climate of southern Thailand, the average summer temperature varies from 35-38°C during the daytime to 27-33°C at nighttime. For the rainy season, the average temperature remains relatively constant at 27-29 °C. The humidity is typically 40-50% during the daytime period and 80-90% at nighttime.

The predicted performance results of concrete bridge piers under the tropical marine environment were determined using field investigation data and the modified time invariant model [46]. For concrete strength, the proposed time variant concrete strength [47] and field data using core testing of the inspected bridges were adopted in the predicted performance model. From the chloride penetration model based on field data, the reference diffusion coefficient and time reduction index were estimated at 100 mm^2/year and 0.325, respectively. Then, the chloride penetration depth ranged from 55 mm to 70 mm over aging periods of 22 to 50 years. From chloride content (0.3 -1.0% weight of cement) with the half-cell potential results ranging from -350 mV to -200 mV, the corrosion rate of steel reinforcement in structural members is estimated to be about 2 mm^2 /year. By using this estimated value, the corrosion rate is incorporated into the modified time invariant model.

The modified time invariant model based on the original residual capacity model [48] is given in Equation 13.

$$f_y(t) = \left(1 - 100\left(\frac{\alpha}{1-0.01Q_{corr}}\right)\left(\frac{A_o - R(t-T_i)}{A_0}\right)\right) f_{yo} \tag{13}$$

where, f_y is the yield strength of the corroded steel rebar, f_{yo} is the yield strength of the non-corroded steel rebar, and α is a force factor that represents the effects of local attack penetration to force, respectively. Q_{corr} is the amount of the reinforcement corrosion (as a percentage). A_0 is the cross-section area of non-corroded reinforcement. Based on field measuring data, the time to corrosion initiation (T_i) is found to be 5.91 years.

To determine structural performance under tropical marine conditions, the predicted interaction relationship between axial load (P) and bending moment (M) was evaluated for aging durations between 5 and 75 years using the proposed modified time invariant model as follows:

$$M(t) = k_1(t)k_3 f_c'(t) b\left(\frac{h}{2} - k_2 c\right) + \sum_{i=1}^{n} F_{si}(t)\left(\frac{h}{2} - d_i\right) \tag{14.1}$$

$$P(t) = k_3 f_c'(t)\left(A_g - A_s(t)\right) + f_y(t)A_s(t) \tag{14.2}$$

$$F_{si}(t) = \begin{bmatrix} \left(f_{si}(t) - k_3 f_c'(t)\right)A_{si}(t) & ;\ 2k_2 c < d_i \\ f_{si}(t)A_{si}(t) & ;\ 2k_2 c > d_i \end{bmatrix} \tag{15.1}$$

$$c = \frac{A_s(t)f_s(t) - A_s'(t)f_s'(t)}{k_1(t)k_3 f_c'(t) b} \tag{15.2}$$

where, A_s and A'_s = reinforcement area in the tension and compression zones, respectively. h = total depth, d = effective depth at each reinforcement level, b = width of cross-section, A_g = gross area of cross-section., k_1 is the ratio of average compressive stress to maximum stress, k_2 is the ratio of distance between the extreme compression fiber and the compression force resultant to the neutral axis depth measured from the extreme compression fiber, and k_3 is the ratio of maximum compressive stress to concrete strength.

The normalized interaction between axial load (P) and bending moment (M) predicted by the modified time variant model indicates that the axial compression and bending capacity are significantly lower than the respective values for the theoretical design model. The reduction is attributed to deterioration in concrete strength and early initiation of steel reinforcement corrosion as shown in Figure 12.

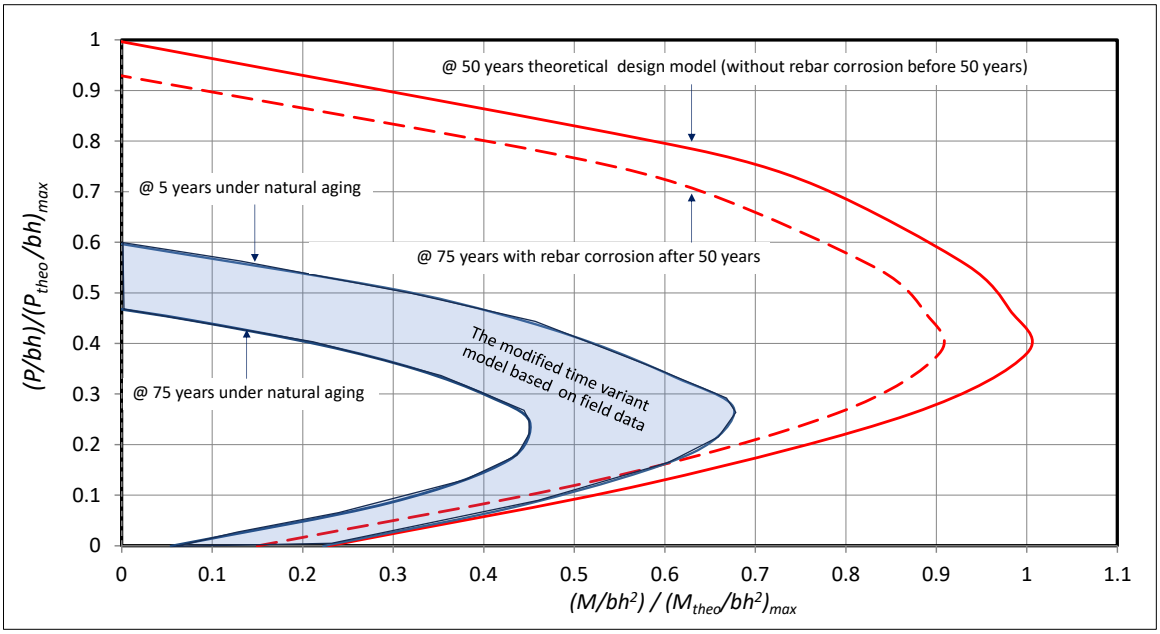

Figure 12. Normalized interaction relations based on the modified time variant model

To determine the correlation between accelerated and natural aging, the predicted axial strength retention versus aging duration based on the proposed modified time invariant model were plotted and compared to outcomes with extrapolated aging cycles as shown in Figure 13. It is observed that the axial strength under the natural aging condition is reduced to 40% of the designed strength within the first five years. After the first five years, the strength reduction will continue gradually, reaching up to 50% over a 60-year period. As compared with the previous study, the predicted results from the modified time variant model are reasonably consistent with those of the research. Hota et al. [49] mentioned that the strength of composites will be degraded by at least 30% in the first three years of service in natural conditions, retaining only 30% of the original strength after 100 years of exposure. In addition, the environmental reduction coefficient of 0.3 has been recommended for incorporation into the design to account for the long-term performance (100-year service life) of GFRP composites under actual field conditions. From correlation in Figure 13, it was found that about 250 and 290 accelerated wet-dry cycles correspond to 0.57 and 0.52 in strength capacity obtained from the theoretical model without reinforcement corrosion, respectively. Therefore, 250 and 290 cycles of accelerated wet-dry aging are equivalent to 25 and 50 years under natural tropical marine conditions. Thus, the knock down factor for GFRP reinforced concrete-filled GFRP tubes (CFFTs) under tropical marine exposure is recommended to be 0.5 for a 50-year design service period.

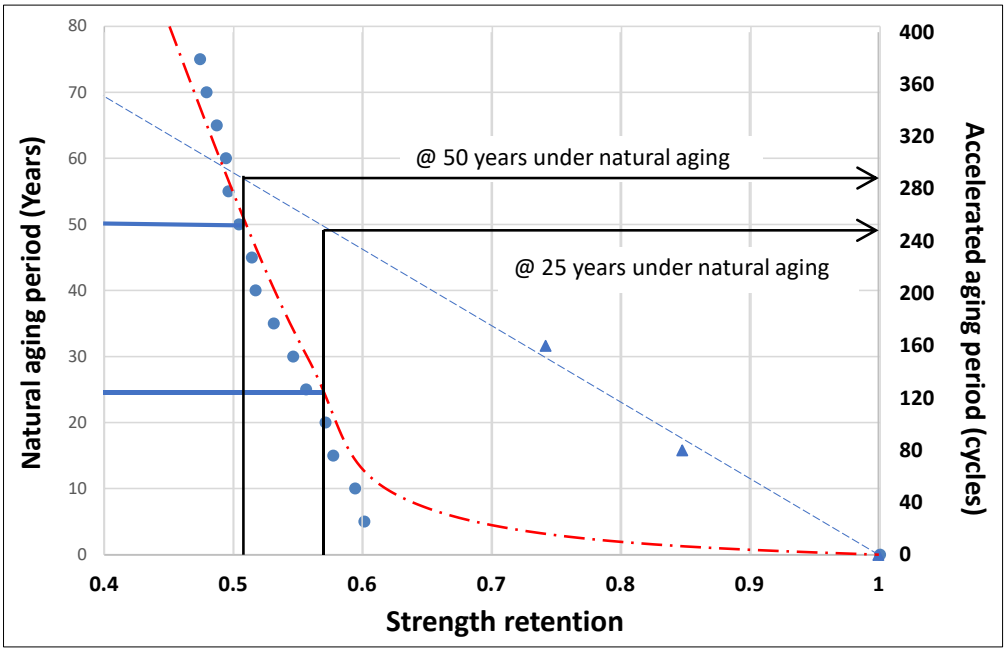

Figure 13. Correlation between accelerated and natural aging

7. Conclusions

GFRP reinforced concrete-filled FRP tubes (CFFTs) under an accelerated wet-dry aging process were experimentally investigated under compression loading to assess structural behavior and performance. Based on experimental and analytical results, the following conclusions are drawn:

- The load and displacement responses still perform in an identical pattern before and after the aging process. Additionally, the failure mode exhibits similar characteristics for column specimens under accelerated aging.
- The average strength ratio (f'_{cc}/f'_c), average lateral strain ratio, and lateral strength decreased with increasing accelerated wet-dry aging duration. However, axial load capacity is minimally affected by the amount of GFRP longitudinal reinforcement. The average deformability factor was determined as 1.055 for both GFRC-F-GFT and C-F-GFT specimens, while GFRC specimens provided a slightly lower value of 1.015.
- The proposed strength model for axial load column capacity incorporating the environmental exposures effect is developed based on the combined strength contribution of different materials. The strength reduction factors according to concrete (C_0) and FRP parts (η_1 and η_2) combined degradation under accelerated wet-dry cycles were proposed as given in Equations 12.1 to 12.3.

Using field data and the modified time invariant model, the correlation between accelerated wet-dry aging and natural tropical marine environment was evaluated through the bridge inspection field data, experimental results and the modified time invariant model. The degradation of column specimens under 290 cycles of accelerated wet-dry aging can reduce axial column capacity up to 50%, equivalent to the degradation under the natural tropical marine environments over 50 years. The knock down factor for GFRP reinforced concrete filled GFRP tubes (CFFTs) under tropical marine exposure is recommended to be 0.5 for a 50-year design service period.

8. Declarations

8.1. Author Contributions

Conceptualization, W.P. and J.O.; methodology, W.P. and J.O.; formal analysis, W.P. and J.O.; investigation, J.O.; writing—original draft preparation, W.P. and J.O.; writing—review and editing, W.P., J.O., A.H., P.I., and O.W.; supervision, W.P. and S.L.; project administration, W.P. and J.O. All authors have read and agreed to the published version of the manuscript.

8.2. Data Availability Statement

The data presented in this study are available on request from the corresponding author.

8.3. Funding and Acknowledgments

The research and publication of this paper were made possible through the financial and facility support provided by the Concrete and Infrastructure Materials Laboratory, Prince of Songkla University, Thailand. The authors gratefully acknowledge this support.

8.4. Conflicts of Interest

The authors declare no conflict of interest.

9. References

[1] Huang, L., Sun, X., Yan, L., & Kasal, B. (2017). Impact behavior of concrete columns confined by both GFRP tube and steel spiral reinforcement. Construction and Building Materials, 131, 438–448. doi:10.1016/j.conbuildmat.2016.11.095.

[2] Tobbi, H., Farghaly, A. S., & Benmokrane, B. (2012). Concrete columns reinforced longitudinally and transversally with glass fiber-reinforced polymer bars. ACI Structural Journal, 109(4), 551–558. doi:10.14359/51683874.

[3] Afifi, M. Z., Mohamed, H. M., & Benmokrane, B. (2014). Axial Capacity of Circular Concrete Columns Reinforced with GFRP Bars and Spirals. Journal of Composites for Construction, 18(1), 04013017. doi:10.1061/(asce)cc.1943-5614.0000438.

[4] Prachasaree, W., Piriyakootorn, S., Sangsrijun, A., & Limkatanyu, S. (2015). Behavior and Performance of GFRP Reinforced Concrete Columns with Various Types of Stirrups. International Journal of Polymer Science, 2015, 1–9. doi:10.1155/2015/237231.

[5] Karim, H., Sheikh, M. N., & Hadi, M. N. S. (2016). Axial load-axial deformation behaviour of circular concrete columns reinforced with GFRP bars and helices. Construction and Building Materials, 112, 1147–1157. doi:10.1016/j.conbuildmat.2016.02.219.

[6] Elchalakani, M., & Ma, G. (2017). Tests of glass fibre reinforced polymer rectangular concrete columns subjected to concentric and eccentric axial loading. Engineering Structures, 151, 93–104. doi:10.1016/j.engstruct.2017.08.023.

[7] Hasan, H. A., Sheikh, M. N., & Hadi, M. N. S. (2019). Maximum axial load carrying capacity of Fibre Reinforced-Polymer (FRP) bar reinforced concrete columns under axial compression. Structures, 19, 227–233. doi:10.1016/j.istruc.2018.12.012.

[8] Wang, J., Feng, P., Hao, T., & Yue, Q. (2017). Axial compressive behavior of seawater coral aggregate concrete-filled FRP tubes. Construction and Building Materials, 147, 272–285. doi:10.1016/j.conbuildmat.2017.04.169.

[9] Bazli, M., Zhao, X. L., Bai, Y., Singh Raman, R. K., & Al-Saadi, S. (2019). Bond-slip behaviour between FRP tubes and seawater sea sand concrete. Engineering Structures, 197, 109421. doi:10.1016/j.engstruct.2019.109421.

[10] Bazli, M., Zhao, X. L., Bai, Y., Singh Raman, R. K., Al-Saadi, S., & Haque, A. (2020). Durability of pultruded GFRP tubes subjected to seawater sea sand concrete and seawater environments. Construction and Building Materials, 245, 118399. doi:10.1016/j.conbuildmat.2020.118399.

[11] Thapa, S., Bazli, M., Ho, T., Le, A., Rajabipour, A., & Hassanli, R. (2025). Enhancing compressive behaviour of seawater sea sand concrete filled hybrid carbon-glass FRP tubes exposed to seawater: Effect of thickness. Engineering Structures, 322, 119052. doi:10.1016/j.engstruct.2024.119052.

[12] Ozbakkaloglu, T. (2013). Compressive behavior of concrete-filled FRP tube columns: Assessment of critical column parameters. Engineering Structures, 51, 188–199. doi:10.1016/j.engstruct.2013.01.017.

[13] Ozbakkaloglu, T., & Vincent, T. (2014). Axial Compressive Behavior of Circular High-Strength Concrete-Filled FRP Tubes. Journal of Composites for Construction, 18(2), 04013037. doi:10.1061/(asce)cc.1943-5614.0000410.

[14] Xue, B., & Gong, J. (2016). Study on steel reinforced concrete-filled GFRP tubular column under compression. Thin-Walled Structures, 106, 1–8. doi:10.1016/j.tws.2016.04.023.

[15] Hadi, M. N. S., Khan, Q. S., & Sheikh, M. N. (2016). Axial and flexural behavior of unreinforced and FRP bar reinforced circular concrete filled FRP tube columns. Construction and Building Materials, 122, 43–53. doi:10.1016/j.conbuildmat.2016.06.044.

[16] Raza, A., Ali, B., & Haq, F. U. (2022). Compressive Strength of FRP-Reinforced and Confined Concrete Columns. Iranian Journal of Science and Technology - Transactions of Civil Engineering, 46(1), 271–284. doi:10.1007/s40996-020-00570-y.

[17] Jing, C., Zhao, L., Chen, S., Wu, T., Chen, Z., & Liu, B. (2025). Experimental and numerical simulation of reinforced concrete-filled GFRP pultruded tubular columns under axial compression. Construction and Building Materials, 462, 139914. doi:10.1016/j.conbuildmat.2025.139914.

[18] Li, Y. L., Zhao, X. L., & Singh Raman, R. K. (2018). Mechanical properties of seawater and sea sand concrete-filled FRP tubes in artificial seawater. Construction and Building Materials, 191, 977–993. doi:10.1016/j.conbuildmat.2018.10.059.

[19] Zhang, B., Sun, J., Zhang, S., Zhou, C., Fan, Z., Yan, Y., & Lin, G. (2024). Compressive behavior of concrete-filled FRP tubes with FRP solid waste as recycled aggregates: Experimental study and analytical modelling. Journal of Building Engineering, 95, 110297. doi:10.1016/j.jobe.2024.110297.

[20] Saadeh, M., & Irshidat, M. R. (2024). Recent advances in concrete-filled fiber-reinforced polymer tubes: a systematic review and future directions. Innovative Infrastructure Solutions, 9(11), 406. doi:10.1007/s41062-024-01722-z.

[21] Elkafrawy, M., Gowrishankar, P., Aswad, N. G., Alashkar, A., Khalil, A., AlHamaydeh, M., & Hawileh, R. (2024). GFRP-Reinforced Concrete Columns: State-of-the-Art, Behavior, and Research Needs. Buildings, 14(10), 3131. doi:10.3390/buildings14103131.

[22] Micelli, F., Mazzotta, R., Leone, M., & Aiello, M. A. (2015). Review Study on the Durability of FRP-Confined Concrete. Journal of Composites for Construction, 19(3), 04014056. doi:10.1061/(asce)cc.1943-5614.0000520.

[23] Elmessalami, N., El Refai, A., & Abed, F. (2019). Fiber-reinforced polymers bars for compression reinforcement: A promising alternative to steel bars. Construction and Building Materials, 209, 725–737. doi:10.1016/j.conbuildmat.2019.03.105.

[24] Taerwe, L. (2020). Compressive behavior of FRP reinforcement in non-prestressed concrete members. Non-Metallic (FRP) Reinforcement for Concrete Structures, CRC Press, Boca Raton, United States. doi:10.1201/9781482271621-42.

[25] Deitz, D. H., Harik, I. E., & Gesund, H. (2003). Physical Properties of Glass Fiber Reinforced Polymer Rebars in Compression. Journal of Composites for Construction, 7(4), 363–366. doi:10.1061/(asce)1090-0268(2003)7:4(363).

[26] Plevkov, V., Baldin, I., Kudyakov, K., & Nevskii, A. (2017). Mechanical properties of composite rebar under static and short-term dynamic loading. AIP Conference Proceedings, 1800, 40018. doi:10.1063/1.4973059.

[27] Li, Y. L., Teng, J. G., Zhao, X. L., & Singh Raman, R. K. (2018). Theoretical model for seawater and sea sand concrete-filled circular FRP tubular stub columns under axial compression. Engineering Structures, 160, 71–84. doi:10.1016/j.engstruct.2018.01.017.

[28] Wang, Z., Zhao, X. L., Xian, G., Wu, G., Singh Raman, R. K., Al-Saadi, S., & Haque, A. (2017). Long-term durability of basalt- and glass-fibre reinforced polymer (BFRP/GFRP) bars in seawater and sea sand concrete environment. Construction and Building Materials, 139, 467–489. doi:10.1016/j.conbuildmat.2017.02.038.

[29] Mohamed, H. M., Afifi, M. Z., & Benmokrane, B. (2014). Performance Evaluation of Concrete Columns Reinforced Longitudinally with FRP Bars and Confined with FRP Hoops and Spirals under Axial Load. Journal of Bridge Engineering, 19(7), 04014020. doi:10.1061/(asce)be.1943-5592.0000590.

[30] Hadhood, A., Mohamed, H. M., & Benmokrane, B. (2017). Axial Load–Moment Interaction Diagram of Circular Concrete Columns Reinforced with CFRP Bars and Spirals: Experimental and Theoretical Investigations. Journal of Composites for Construction, 21(2), 04016092. doi:10.1061/(asce)cc.1943-5614.0000748.

[31] ACI 318-08. (2008). Building code requirements for structural concrete and commentary. American Concrete Institute (ACI), Farmington Hills, United States.

[32] ACI 318-11. (2011). Building code requirements for structural concrete and commentary. American Concrete Institute (ACI), Farmington Hills, United States.

[33] CSAS806–12. (2012). Design and construction of building components with fiber reinforced polymers. Canadian Standards Association (CSA), Toronto, Canada.

[34] AS 3600:2018. (2018). Australian Standard for Concrete Structures. Standards Association of Australia, Sydney, Australia.

[35] Saafi, M., Toutanji, H. A., & Li, Z. (1999). Behavior of concrete columns confined with fiber reinforced polymer tubes. ACI Materials Journal, 96(4), 500–509. doi:10.14359/652.

[36] Lam, L., & Teng, J. G. (2003). Design-oriented stress-strain model for FRP-confined concrete. Construction and Building Materials, 17(6–7), 471–489. doi:10.1016/S0950-0618(03)00045-X.

[37] Matthys, S., Toutanji, H., Audenaert, K., & Taerwe, L. (2005). Axial load behavior of large-scale columns confined with fiber-reinforced polymer composites. ACI Structural Journal, 102(2), 258. doi:10.14359/14277.

[38] Wu, Y.-F., & Wang, L.-M. (2009). Unified Strength Model for Square and Circular Concrete Columns Confined by External Jacket. Journal of Structural Engineering, 135(3), 253–261. doi:10.1061/(asce)0733-9445(2009)135:3(253).

[39] Park, J. H., Jo, B. W., Yoon, S. J., & Park, S. K. (2011). Experimental investigation on the structural behavior of concrete filled FRP tubes with/without steel re-bar. KSCE Journal of Civil Engineering, 15(2), 337–345. doi:10.1007/s12205-011-1040-0.

[40] Realfonzo, R., & Napoli, A. (2011). Concrete confined by FRP systems: Confinement efficiency and design strength models. Composites Part B: Engineering, 42(4), 736–755. doi:10.1016/j.compositesb.2011.01.028.

[41] Ozbakkaloglu, T., Lim, J. C., & Vincent, T. (2013). FRP-confined concrete in circular sections: Review and assessment of stress-strain models. Engineering Structures, 49, 1068–1088. doi:10.1016/j.engstruct.2012.06.010.

[42] Robert, M., & Benmokrane, B. (2013). Combined effects of saline solution and moist concrete on long-term durability of GFRP reinforcing bars. Construction and Building Materials, 38, 274–284. doi:10.1016/j.conbuildmat.2012.08.021.

[43] Zaman, A., Gutub, S. A., & Wafa, M. A. (2013). A review on FRP composites applications and durability concerns in the construction sector. Journal of Reinforced Plastics and Composites, 32(24), 1966–1988. doi:10.1177/0731684413492868.

[44] ACI440.2R-17 (2017) Guide for the design and construction of externally bonded FRP systems for strengthening concrete structures. Reported by ACI Committee 440, American Concrete Institute (ACI), Farmington Hills, United States.

[45] CSA S6-14. (2005). Canadian Highway Bridge Design Code. Canadian Standards Association (CSA), Toronto, Canada.

[46] Prachasaree, W., Limkatanyu, S., Wangapisit, O., & Kraidam, S. (2018). Field Investigation of Service Performance of Concrete Bridges Exposed to Tropical Marine Environment. International Journal of Civil Engineering, 16(12), 1757–1769. doi:10.1007/s40999-017-0250-3.

[47] Niu, Y.-Z., Tu, C.-L., Liang, R. Y., & Zhang, S.-W. (1995). Modeling of Thermomechanical Damage of Early-Age Concrete. Journal of Structural Engineering, 121(4), 717–726. doi:10.1061/(asce)0733-9445(1995)121:4(717).

[48] Du, Y. G., Clark, L. A., & Chan, A. H. C. (2005). Residual capacity of corroded reinforcing bars. Magazine of Concrete Research, 57(3), 135–147. doi:10.1680/macr.57.3.135.60482.

[49] Hota, G., Barker, W., & Manalo, A. (2020). Degradation mechanism of glass fiber/vinylester-based composite materials under accelerated and natural aging. Construction and Building Materials, 256, 119462. doi:10.1016/j.conbuildmat.2020.119462.